Article

pubs.acs.org/Biomac

Poly(ethylene glycol) Conjugation Stabilizes the Secondary Structure of α-Helices by Reducing Peptide Solvent Accessible Surface Area

Elham Hamed,[†] Ting Xu,[‡] and Sinan Keten*[,†]

[†]Department of Civil and Environmental Engineering and Department of Mechanical Engineering, Northwestern University, Evanston, Illinois 60208, United States

[‡]Department of Materials Science and Engineering, University of California, Berkeley, California 94720, United States

Supporting Information

ABSTRACT: We investigate the effect of poly(ethylene glycol) (PEG) side-chain conjugation on the conformational behavior of an α-helix using molecular dynamics simulations in explicit solvents of varying hydrophobicity. Our simulations illustrate an increase in peptide helicity with increasing PEG molecular weight in the range ∼400 to 1800 Da. The data with varying PEG contour lengths as well as constant force pulling simulations that allow control over the end-to-end length of PEG indicate a strong inverse correlation between peptide helicity and solvent accessible surface area (SASA). A residue-based mapping analysis reveals that the formation of a protecting PEG shell around peptide helix in water is facilitated by two distinct mechanisms that depend on the solvent environment. First, cationic residues such as lysine interact favorably with PEG due to strong polar interactions with PEG oxygen atoms. Additionally, we find that hydrophobic residues interact strongly with PEG to reduce their SASA in polar solvents by polymer shielding. Our simulations illustrate that these two mechanisms that involve side-chain chemistry and solvent polarity govern the preferred conformation of PEG on the helix surface and thus the stability of peptide secondary structure. These findings elucidate the molecular mechanisms underpinning recent experimental findings on the stability and conformational dynamics of protein−PEG conjugates.

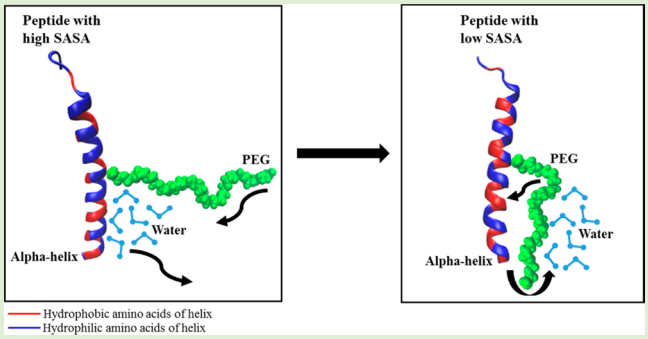

INTRODUCTION

α-Helices are among the most common and stable protein secondary structures in nature. Unstructured short polypeptide sequences in aqueous solution experience a competition between peptide−water and peptide−peptide interactions, which is resolved when local backbone hydrogen bonds stabilize this universal helical fold.[1] Apart from their numerous functions in biology, α-helices have emerging applications as vehicles for drug delivery and bioactive polymer functional groups.[2−6] However, the desirable functionalities of α-helices are dependent upon their structural stability,[7] which can be lost during fabrication, handling, storage, and service lifetime of engineered materials that involve extreme and nonphysiological environmental conditions, such as very high temperatures, pressures, or pH.[8−11] Small peptides consisting of short helices generally have low structural and thermal stability[12] and constitute a challenging benchmark system for studying strategies for increasing α-helix stability.

Earlier studies have shown that helix stability can be improved by increasing the hydrophobicity of the peptide hydrophobic core,[13−15] helix capping,[16,17] use of hydrogen-bond surrogates,[18,19] use of hydrocarbon staples,[20−22] or introducing specific interstrand interactions such as salt bridges,[23−25] lactam bridges,[26−29] and disulfide bonds.[30−32] Recently, conjugation of α-helices with poly(ethylene glycol) (PEG) has been utilized to produce environmentally responsive block copolymers with improved properties, such as increased stability, improved aqueous solubility, and tailored functionalities.[33−36] The majority of reported peptide−PEG conjugates were constructed by covalently linking PEG to one of the peptide terminal amino acids to form linear peptide-PEG block copolymers.[6,35,37,38] However, this architecture was shown to decrease the mechanical and thermal stability of short peptides,[35,38] possibly due to the entropic penalty of the conjugation, thermal oscillations of the attached domain, or unwinding of the ends of the helices. The destabilizing effect becomes more noticeable for smaller peptides and longer polymer chains and high pH conditions.[39,40] Recently, Shu et al.[39] presented a new design in which the PEG chain was covalently attached to the sides of the coiled coil bundle. This architecture reduces steric occlusion and, therefore, enhances the mechanical and thermal stability of the structure and retains the peptide secondary and tertiary structure.[39,41]

While there have been numerous experiments that showed stabilization of peptides with PEG conjugation,[6,35,37−40] the underlying mechanisms of stabilization remain to be fully

Received: August 4, 2013
Revised: September 6, 2013
Published: September 16, 2013

understood. In particular, the coupling between peptide, polymer, and solvent interactions makes it challenging to discern the factors that lead to protein stabilization in experiments. Molecular and mesoscale simulations that elucidate peptide−PEG conjugate conformational dynamics in different solvent environments have remained missing in the literature, and are necessary to provide a comprehensive picture of the mechanisms underpinning stabilization through PEG conjugation. Quantification of the radius of gyration of PEG in different solvents and how PEG modulates peptide-solvent interactions is crucially important for understanding helix stability and higher order assemblies. As a first step toward quantifying these effects, here we perform atomistic and coarse-grained (CG) simulations of an α-helix side-conjugated with PEG in different solvent environments. As a model system, we take the helix−PEG conjugates previously synthesized and characterized experimentally by Shu et al.[39] Based on this model, we first perform all-atom simulations of peptide−PEG conjugates with different PEG molecular weights to investigate the correlation between peptide helicity, peptide solvent accessible surface area, and PEG chain length. Next, we build CG models of the peptide−PEG conjugate systems and study PEG conformations to generalize our observations to polar and nonpolar solvent environments, specifically including water, acetone, and chloroform as possible scenarios. Predictions of the all-atom and CG models are validated by comparisons of PEG radius of gyration with experimental data. The conformations of PEG radially from the helix axis as well as axially along the helix length are characterized to correlate solvent accessible surface area with helix stability.

MATERIALS AND METHODS

Materials. The peptide structure was built based on an α-helical peptide that has 28 amino acids (pdb id "1coi" in the protein data bank[42]). Five more amino acids, Gly-Trp-Asp-Gly-Arg, were added to the N-terminus of the original peptide, where cell-adhesion functionality was studied, following ref 39. The serine at the middle of peptide was mutated to cysteine to facilitate the attachment of maleimide-capped PEG through formation of a carbon−sulfur bond. The schematic of peptide−PEG conjugate is shown in Figure 1a. The conjugated PEG chains had a fully extended configuration in the initial structure. PEG chains with four different molecular weights were used to construct peptide−PEG conjugates: 442, 882, 1323, and 1763 Da with, respectively, 10, 20, 30, and 40 PEG monomers. We refer to these PEG chains as PEG10, PEG20, PEG30, and PEG40 throughout the manuscript.

All-Atom Simulations. All-atom simulations were performed using NAMD.[43] The peptide−PEG conjugate was solvated in a water box, with 15 Å padding and periodic boundary conditions in the three dimensions, using the TIP3P water model.[44] The equations of motion were solved using the velocity Verlet algorithm with a time step of 1 fs. NPT ensemble with constant pressure of 1 atm and constant temperature of 300 K was adopted for the simulations. Bonded interactions of peptide and PEG were modeled using the CHARMM force field and those of maleimide were estimated using CHARMM General Force Field (CGenFF).[45] Long-range interactions were computed using standard Lennard-Jones potentials and the particle mesh Ewald technique for electrostatics. The minimization of the peptide−PEG conjugate systems for 15000 steps was followed by a 40 ns equilibration simulation. Figure 1b illustrates a snapshot of the all-atom simulation of an equilibrated helix−PEG conjugate. The equilibration of the systems was ensured by monitoring the convergence of several system parameters, including potential energy, peptide helicity, peptide solvent accessible surface area, and PEG radius of gyration. It should be noted that one initial configuration and a single simulation were run for each individual peptide−PEG conjugate. The reported results for all cases represent the simulation time-averages, and the corresponding error bars pertain to time-associated standard deviations.

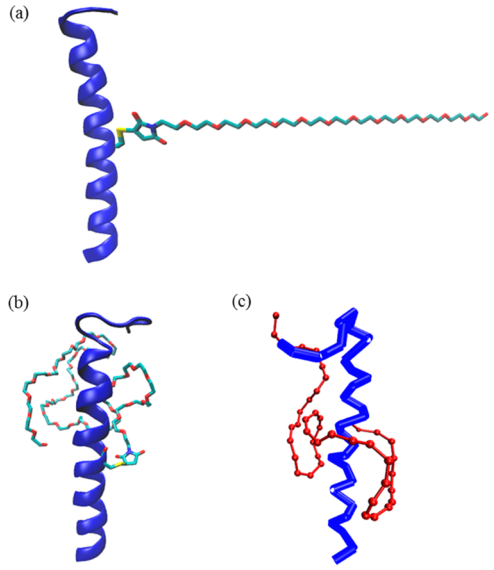

Figure 1. (a) Schematic of the initial structure of peptide−PEG conjugate, with the PEG chain attached to the cysteine side chain approximately at the midspan of the α-helix. The peptide has a sequence of Ac-EVEALEKKVAALECKVQALEKKVEALEHGWDGR-$CONH_2$. Simulation snapshots of (b) all-atom and (c) coarse-grained helix−PEG conjugate models.

To quantify the stability of the peptide in all-atom simulations, fractional helicity was calculated from the simulation trajectories. Fractional helicity is defined as the time-averaged number of residues with helical secondary structure divided by the total number of peptide residues. The STRIDE algorithm implemented in VMD[46] was used to quantify the secondary structure.

Constant force pulling simulations were also performed on a solvated peptide-PEG system with PEG molecular weight of 882 Da (PEG20). This molecular weight, which is an intermediate one among all the studied weights, was selected as an example case study to validate our hypothesis. To that end, a fictitious spring was attached to the PEG chain, from its beginning to the end, and was pulled with a constant force to keep the PEG chain in a desirable extension state. We examined cases with varying constant tension forces of 0, 0.1, 1, and 4 kcal/mol/Å on the PEG chain. These cases are bounded by two extreme values: (i) the spring force is zero and PEG is completely free to move around peptide and (ii) the spring force is high enough to keep the PEG chain completely extended and, therefore, away from peptide. All the applied pulling forces were selected such that they do not generate dynamic perturbations that could make the peptide unfold.

Coarse-Grained Simulations. Coarse-grained models were built and run using NAMD with MARTINI force field,[47,48] with bead definition and force field parameters for PEG being taken from ref 49. The CG peptide−PEG conjugate was solvated in a CG water box with periodic boundary conditions in all directions. To avoid freezing of MARTINI water at the simulated temperatures,[50,51] 10% of water was replaced with antifreeze particles, as suggested in the original model.[48] To study the effect of solvent on the behavior of the peptide−PEG conjugate, two other solvents were also employed: acetone and chloroform. The only difference between the modeled solvents was the type of employed MARTINI bead and, consequently, the effective interaction energy, ε, between the CG beads. For water, ε was set to 1.195 kcal/mol, while for acetone and chloroform it was taken as 0.956 and 0.836 kcal/mol, respectively.[48] Changing the value of ε primarily changes the hydrophobicity of CG solvents, with the hydrophobicity increasing from water to acetone to chloroform. We note that the CG

models used here are not validated models for the specific solvents, rather they are used here merely as a proxy for the role of hydrophobicity specifically on PEG conformation. No antifreeze particles were used in the case of acetone and chloroform. Throughout the simulations, the pressure was maintained at 1 bar and temperature at 300 K. A time step of 5 fs was used to integrate the equations of motion. The CG simulations were performed for ∼100 ns. Figure 1c shows a snapshot of the CG simulation of an equilibrated peptide−PEG conjugate. The criteria for checking the equilibration of CG systems were similar to those of all-atom models mentioned in the previous section.

Solvent Accessible Surface Area Analysis. One important parameter correlated with helix stability is the solvent accessible surface area (SASA). SASA is the area of the surface sought by rolling a probe sphere, representing the solvent, over the surface of the peptide. The area that is accessible to the probe and does not overlap with the neighboring particles is exposed to the solvent, and thus is considered as solvent accessible. SASA analysis was performed using an algorithm implemented in VMD.[46] In all-atom simulations, a probe radius of 1.4 Å was employed to approximate the van der Waals radius of a water molecule. The probe radius was assumed to be 2.6 Å in CG calculations, which is close to van der Waals radius of CG beads of the employed solvents, namely, water, acetone, and chloroform. It should be noted that many factors, including the choice of probe radius, affect the SASA measurements, but should not change the trends observed in this study.

RESULTS AND DISCUSSION

Here we present atomistic and coarse-grained simulation results on the behavior of peptide−PEG conjugates. First, we analyze the effect of polymer conjugation using all-atom simulations that are capable of capturing conformational transitions within the peptide. Figure 2 shows the average fractional helicity of the peptide for different PEG molecular weights obtained from all-atom simulations in comparison with experimental measurements[39] at 300 K. Our simulations indicate that an increase of ∼9.5% in peptide helicity is possible by increasing the PEG molecular weight from 442 to 1763 Da. This finding is in very good agreement with experimental data that shows an increase of ∼15% in peptide helicity with increasing PEG molecular weight from 750 to 2000 Da.[38] The obtained results suggest that the attachment of PEG does not cause unfolding of the peptide at any molecular weight in the range studied. On the contrary, conjugation with PEG stabilizes the secondary structure of the helix and enhances its helicity to a greater extent with increasing PEG molecular weight. This behavior has been observed both in experiments[39] and simulations[41] for side-conjugated helix−PEG constructs. Our all-atom simulations in explicit water further reveal that stabilization involves an increase in backbone hydrogen bonds (Hbonds). This agreement between experiment and simulation validates the basic features of our modeling and simulation approach, which we use further to carry out analyses on molecular mechanisms.

All-atom simulations clearly show that the helix does not unfold due to PEG conjugation (Figure 2). This motivates the use of simpler CG models that preserve the helical secondary structure while extending the time and length scales of observation to assess conformational changes of PEG in different solvents. To validate the CG model, we compare the radius of gyration of PEG obtained from CG simulations with that of all-atom models as well as experiments in water solvent. CG and all-atom radii of gyration given in Figure 3a show a very good agreement for all PEG molecular weights studied. The errors associated with all-atom and CG calculations of R_g in water are reported in Table S1 of the Supporting Information. Additionally, the scaling of R_g with molecular weight (Figure 3a) yields the relationships $R_g \propto M_w^{0.462}$ and $R_g \propto M_w^{0.471}$ for all-atom and CG simulations respectively, showing very good agreement. Experimental data for unattached PEG in water shows that $R_g \propto M_w^{\nu}$, where $\nu = 0.505 \pm 0.004$ for $M_w < 2000$ and $\nu = 0.571 \pm 0.001$ for $2000 < M_w < 7500$.[49,52] Given that all the PEG chains employed in the current study have molecular weights less than 2000 Da, the

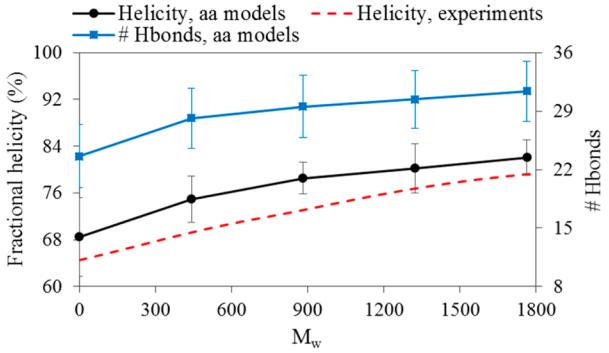

Figure 2. Fractional helicity of the peptide as a function of PEG molecular weight (M_w; black solid circle markers). Predictions are based on all-atom (aa) molecular dynamics simulations and are compared with the experimental data from ref 39 (dashed red line, no markers). The secondary axis (blue solid square markers) illustrates the number of backbone hydrogen bonds (H bonds) for helix−PEG conjugates with different PEG molecular weights.

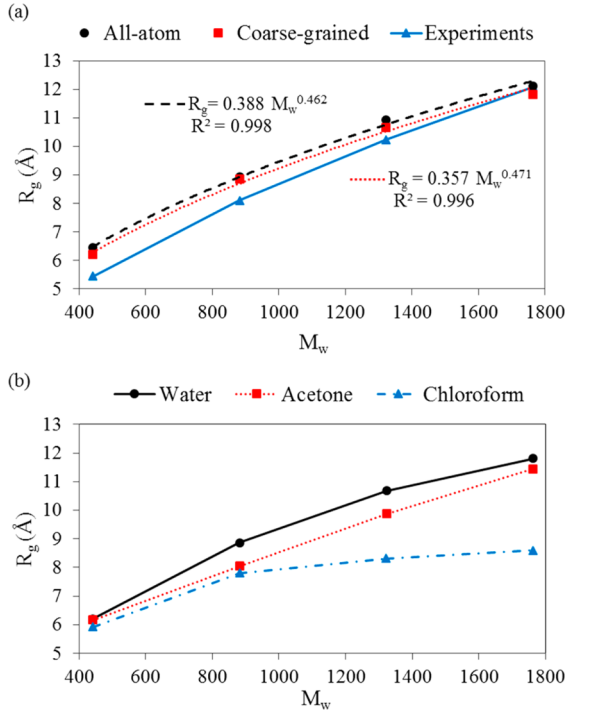

Figure 3. (a) Comparison between the radius of gyration (R_g) of PEG chains attached to an α-helix computed from all-atom vs coarse-grained simulations in explicit water as well as their comparison with experimental results of ref 53. Scaling of R_g with the PEG molecular weight (M_w) in water is close to the ideal chain behavior, and (b) the effect of different solvents on PEG R_g obtained by coarse-grained modeling.

dx.doi.org/10.1021/bm401164t | Biomacromolecules 2013, 14, 4053−4060

obtained all-atom and CG modeling scaling laws are in very good agreement with experimental observations. Figure 3a also includes the PEG radius of gyration obtained experimentally[53] for a peptide-PEG system solvated in water, which is close to the all-atom and CG modeling predictions.

In general, the conformation and M_w scaling of the PEG chain depend on the solvent environment. To generalize these findings to different solvent conditions, we employ the CG models to study the effect of different organic solvents on the behavior of peptide−PEG conjugate systems. The results, given in Figure 3b, show a decrease in R_g with decreasing solvent polarity, from water to acetone to chloroform. This is because the hydrophilic PEG chain collapses to minimize its own solvent accessible area in increasingly hydrophobic solutions. It should be noted that the CG models were only validated for water and not the other solvents. However, the trends observed clearly illustrate how good vs bad solvents will change conformations of PEG on peptide surfaces.

Previous studies[39,41] and the current one have reported an increase in peptide helicity upon side-chain PEG conjugation. However, the mechanism underlying the stabilization effect of PEG chains on the peptide is not yet fully understood. Since the stability observations generally hold for various peptide-PEG systems studied to date,[37,39,40,54−58] we hypothesize that PEG conjugation increases the helix stability specifically by forming a shielding shell around it, thereby reducing the solvent accessible surface area of the peptide. To prove this hypothesis, we first quantify SASA of the peptide for PEG chains of different molecular weights. Figure 4 shows an inverse

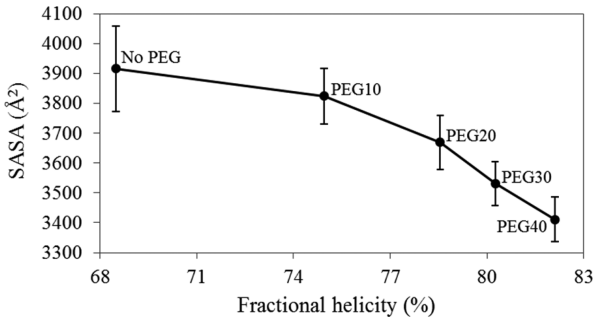

Figure 4. Solvent accessible surface area (SASA) of the peptide as a function of its helicity, as predicted by all-atom simulations of helix−PEG conjugates with PEG chains of different lengths in water. As the length (or molecular weight) of the conjugated PEG increases, the fractional helicity increases significantly, whereas the SASA decreases. The data thus suggests an inverse correlation between the SASA of the peptide and its fractional helicity, supporting the hypothesis that protection from the solvent and favorable interactions of the PEG with the peptide enhance the helix stability.

relationship between the SASA of the peptide in water and both peptide helicity and PEG molecular weight. Each data point in this figure represents the simulation time-average value of SASA and its error bar corresponds to the time-associated standard deviation. The data shows that higher M_w chains are more effective in reducing the SASA and consequently increasing the stability of the α-helix.

We use an alternative approach to validate our hypothesis that SASA governs helix stability and to ascertain that other factors such as the added mass of the PEG are not the primary factors leading to a greater helicity. To that end, the PEG extension state is controlled through constant force pulling simulations, as shown schematically in Figure 5a, and the peptide helicity and SASA are quantified for different PEG end-

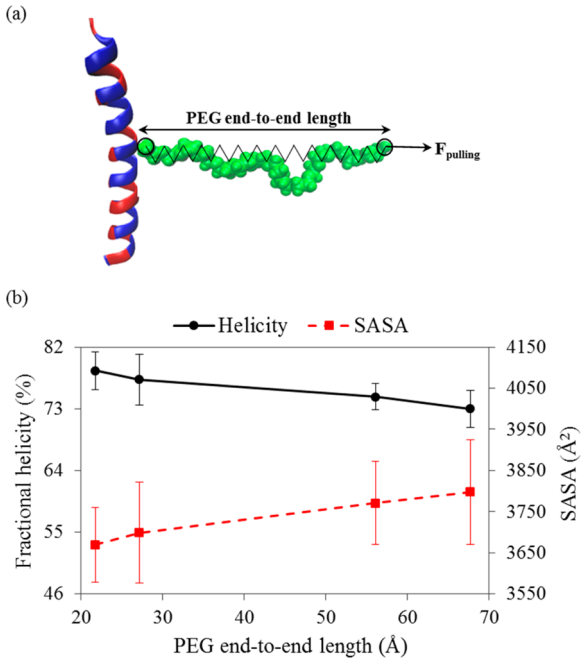

Figure 5. (a) Schematic of constant force pulling simulations in which the PEG chains are extended to different end-to-end lengths by the application of an external bias force, $F_{pulling}$, and (b) peptide helicity and solvent accessible surface area (SASA) as a function of PEG end-to-end length for a peptide−PEG conjugate with PEG molecular weight of 882 Da (PEG20). Independent of the solvent environment, extended PEG chains expose more of the helix surface to the solvent. Consequently, a monotonic decrease in helicity is observed for the cases studied here.

to-end lengths. The simulation results (Figure 5b) suggest that as the PEG end-to-end length increases, the peptide SASA increases, which makes the backbone hydrogen bonds more accessible to water attacks and thus the peptide helical content decreases. In conclusion, data from constant force simulations as well as M_w studies consistently suggest that there exists an inverse correlation between peptide helicity and its solvent accessible surface area. Both chemical and mechanical factors that lead to an increase in SASA are observed to lead to a destabilizing effect on the peptide.

Now that SASA is determined as a key factor that correlates well with helix stability, the key question to be asked is how the choice of the solvent and the peptide sequence play a role on the conformation of PEG near the peptide surface. To shed light on this issue, here we first quantify how PEG conjugation changes the SASA of peptide residues in solvents with different polarities. Figure 6 illustrates the SASA of the hydrophobic and hydrophilic segments of the peptide for different solvents and different PEG molecular weights. The hydrophobic segment includes all the amino acids with hydrophobic side chains in the peptide sequence, namely, Val, Leu, Ala, Trp, and Gly, whereas the hydrophilic segment represents all the other amino acids. The CG simulation results predict that as the polarity of solvent decreases, the SASA of hydrophobic amino acids increases, while the SASA of hydrophilic residues decreases. This contrasting effect of the solvent on different residues can be explained as follows. When the solvent is hydrophobic, the

dx.doi.org/10.1021/bm401164t | Biomacromolecules 2013, 14, 4053−4060

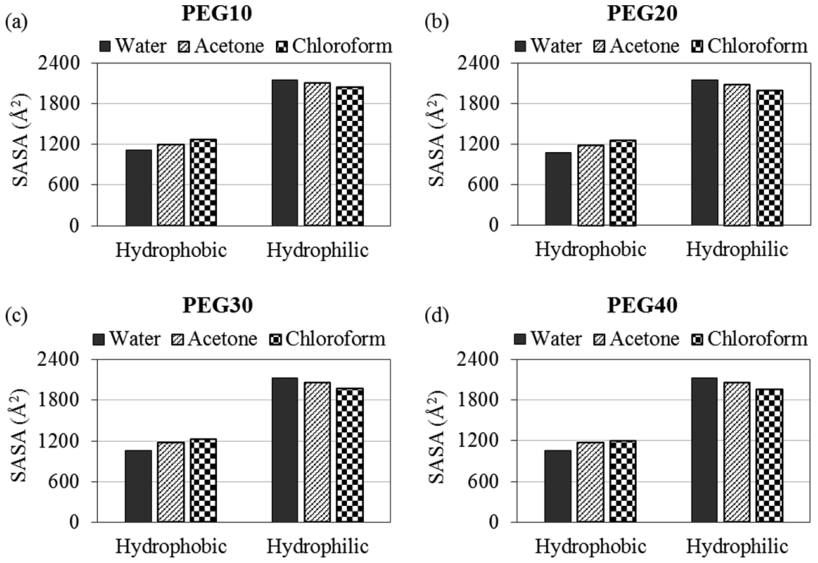

Figure 6. Solvent accessible surface area (SASA) of the hydrophobic and hydrophilic segments of the peptide obtained for different solvents and different PEG molecular weights of (a) PEG10, (b) PEG20, (c) PEG30, and (d) PEG40. All the results are predicted by coarse-grained simulations. The data suggests that increasing the hydrophobicity of the solvent (going from water to acetone, and then to chloroform, which is the most hydrophobic of the three) causes PEG chains to collapse onto the hydrophilic regions of the peptide, leaving hydrophobic regions more exposed to the solvent.

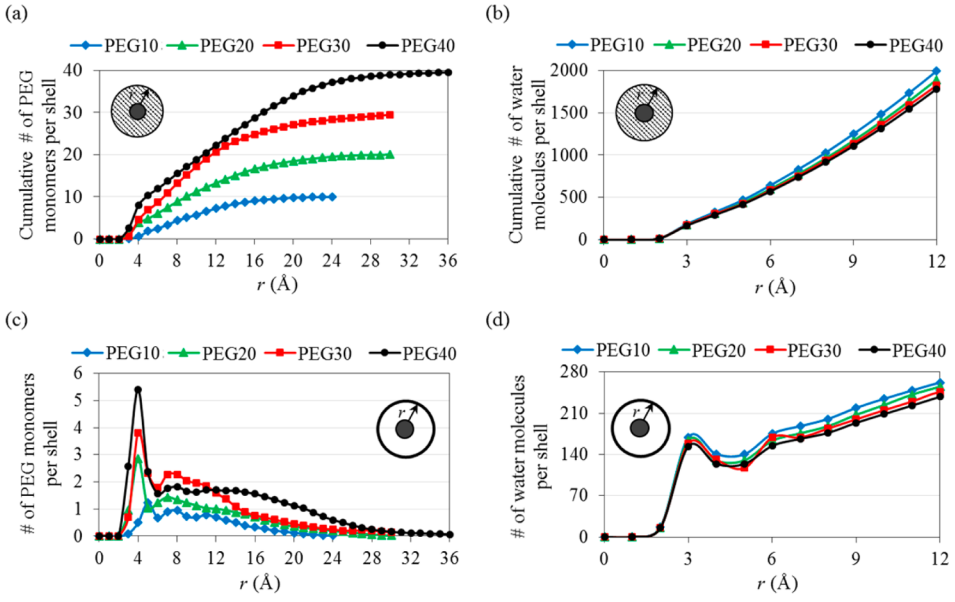

Figure 7. Cumulative number of (a) PEG monomers and (b) water molecules within a shell of radius r around peptide, as well as number of (c) PEG monomers and (d) water molecules at radial distance r from the peptide for PEG chains of different molecular weights. These results pertain to all-atom simulations. As the PEG molecular weight is increased, the overall density of PEG monomers in the vicinity of the peptide increases while the density of water decreases, leading to a decrease in the overall SASA of the peptide.

solvation penalty of the hydrophilic residues is very high, and the PEG chain adopts conformations to minimize this penalty by covering the exposed hydrophilic regions. This allows for the more hydrophobic regions of the peptide to have greater exposure to the solvent. The solvent exposure of all residues generally shows a dependence on the molecular weight of PEG as well. Specifically, the SASA of both hydrophobic and hydrophilic parts decrease slightly with increasing PEG molecular weight, implying that the peptide surface globally becomes less accessible to solvent for longer PEG chains.

To shed light on the mechanisms underlying peptide-PEG interactions, we use all-atom models to quantify the radial and cumulative number of PEG monomers as a function of the radial distance from the helix axis. The results, given in Figure 7a,c, show that, for longer PEG chains, there exist more PEG monomers closer to the peptide. Additionally, Figure 7b,d shows the results of a similar analysis for the number of water molecules in the proximity of peptide. As the length of the attached PEG chain increases, the overall density of water molecules surrounding the peptide decreases, in agreement with an increase in the PEG density illustrated in Figure 7a,c. These observations explain experimental results by clearly illustrating that longer PEG chains are more effective in forming a large shell in the vicinal layers of the peptide, which

dx.doi.org/10.1021/bm401164t | *Biomacromolecules* 2013, 14, 4053−4060

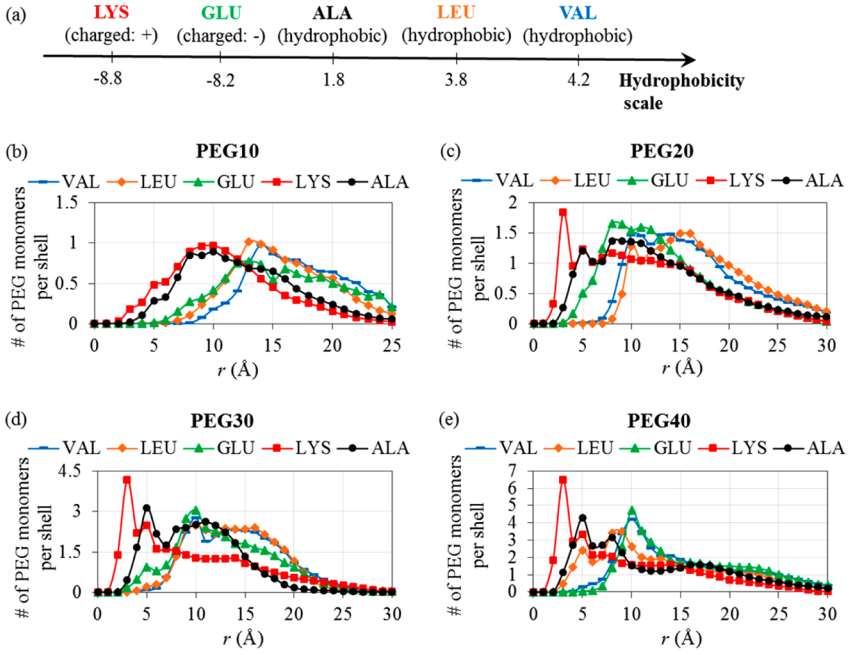

Figure 8. (a) Characteristics and hydrophobicity scale of the amino acids valine (Val), leucine (Leu), alanine (Ala), glutamic acid (Glu), and lysine (Lys) employed in the analysis of distribution of PEG monomers at radial distance r from the mentioned amino acids for PEG chains of different molecular weights: (b) PEG10, (c) PEG20, (d) PEG30, and (e) PEG40. The results pertain to all-atom simulations and the selected residues are the ones that show the greatest amount of interaction with the PEG chain, as quantified by the number of PEG monomers in their vicinity. The results clearly illustrate that the positively charged residue Lys and slightly hydrophobic residue Ala interact strongly with the PEG chains, showing monomer centers at close proximity to these residues. More hydrophobic residues such as Val and Leu also show close proximity to PEG chains, but not as much as the smaller Ala residue. Negatively charged residue GLU follows a similar trend to VAL, and exhibits less interaction with the PEG chain compared to the positively charged Lys. These results can be explained on the basis of the relative solvation penalty of the residues and the tendency for PEG oxygens to interact with cationic charged residues.

stabilizes the secondary structure of peptide by shielding the peptide hydrogen bonds from water attacks.

Figure 7 gives some insights on how PEG chains interact with the peptide radially; however, it cannot explain the interaction between PEG and different amino acids along the peptide length. To identify which amino acids have the strongest interaction with PEG, we calculate the cumulative distribution of PEG monomers in the vicinity of every amino acid separately. The results, listed in Tables S2 and S3 of the Supporting Information, suggest that, first, the PEG does not interact much with the amino acids at the two ends of peptide. Especially the PEG interaction with far end of the peptide, which has the five amino acids Gly-Trp-Asp-Gly-Arg, is almost zero. This behavior, which holds for all four PEG molecular weights studied, is most likely due to the fact that PEG is attached close to the middle section of the peptide, which provides proximity to central regions more than the peptide termini. Among the amino acids that the PEG chain has access to, it mainly interacts with the amino acids lysine (Lys), alanine (Ala), glutamic acid (Glu), valine (Val), and leucine (Leu). It should be noted that these are the most occurring amino acids in the peptide sequence with Lys, Ala, Glu, Val, and Leu, comprising, respectively, 5, 5, 7, 4, and 4 residues of the total 33 peptide residues. Among the mentioned amino acids, PEG has the least amount of interaction with the amino acids Val and Leu, which are the hydrophobic residues located, respectively, in the *a* and *d* positions of the peptide heptad repeat. The strongest PEG interactions, as indicated by the largest occurrence of PEG monomers in the vicinity of the residues, are observed for Lys, Ala, and Glu, in order. Lys and Glu are the charged amino acids located in the *e* and *g* positions of the heptad that form a salt bridge in coiled coils. Figure 8 summarizes these findings, where the number of PEG monomers as a function of radial distance are shown separately for the amino acids Val, Leu, Glu, Lys, and Ala for different PEG molecular weights. In this figure, the reported result for each amino acid represents the total number of PEG monomers summed up over all the amino acids of the same type present in the peptide sequence. These results confirm that, for all PEG molecular weights, PEG and Lys have the strongest interaction (the first peak in the curves). As the PEG chains become longer, the magnitude of the Lys peak becomes larger and it occurs at a location closer to the peptide. Therefore, the cationic Lys side chain provides a potential preferred site for PEG oxygens, which contributes to the formation of a PEG shell around peptide and its corresponding stabilization effect. This behavior, namely, the strong interaction between charged residues, especially Lys, and PEG, was also reported in other studies.[41,59] In this study, we show that this finding is valid for a range of different PEG molecular weights and most importantly, we illustrate the importance of PEG interactions with other amino acids, which cumulatively have a favorable energetic effect that contributes to PEG stabilization effect. After Lys, the amino acid Ala has the closest radial distribution peak to the peptide. The magnitudes of peaks of other amino acids, namely, Glu, Leu, and Val, are about the same as that of Ala, but they occur at slightly further distances from the peptide.

The most important observation from this study is that the hydrophobic residues also interact strongly with PEG, which supports our hypothesis that PEG interaction with the surface depends not only on the strength of the helix−PEG

dx.doi.org/10.1021/bm401164t | *Biomacromolecules* 2013, 14, 4053−4060

interactions alone, but also the solvation penalty of the residues, which is higher for hydrophobic residues. Thus, the energetic gain of protection that PEG provides becomes more favorable for these residues than others in polar solvents. These findings and the observations from Figure 6, which illustrate the peptide SASA in different solvent environments, suggest that solvent polarity serves as a fulcrum point that can drastically change the conformation of PEG on the peptide surfaces. Based on these findings, it is foreseeable to utilize polymer conjugation as a tool for enabling peptide secondary structure stabilization in otherwise unfavorable organic solvents.

CONCLUSIONS

In this study, we perform all-atom and coarse-grained simulations of α-helices side-chain conjugated with PEG, to gain some insight into the molecular mechanisms underpinning stability of peptide-PEG conjugates, as validated by experimental observations.[38−40,53] In particular, our investigations clearly indicate an increase in peptide fractional helicity with an increase in PEG molecular weight, in agreement with previous studies.[39,41] We show that this trend correlates well with the presence of a more effective PEG shell around the peptide that (i) reduces the peptide solvent accessible surface area, and thus protects the backbone hydrogen bonds from solvent attacks; and (ii) reduces interfacial energy for hydrophobic domains exposed to a polar solvent. The validity of this hypothesis is confirmed by calculations of SASA of peptide in water, which shows an inverse relationship with both peptide helicity and PEG molecular weight. Additionally, simulations of peptide−PEG conjugates in which the PEG chain is pulled to different end-to-end lengths through the application of a constant tension force confirm an inverse correlation between peptide SASA and helicity. Based on these observations, we conclude that chemical as well as mechanical factors that lead to a decrease in SASA of peptide will generally lead to an increase in helix stability.

The predicted radial distribution of PEG chains in the proximity of peptide, which shows existence of a larger number of PEG monomers closer to the peptide for longer PEG chains, proves that shielding effect of PEG on helix-solvent interactions to minimize the water attacks on peptide hydrogen bonds is a key mechanism contributing to the improved stability of α-helices upon PEG conjugation. Additionally, our residue-based mapping analysis reveals that the formation of a shielding PEG shell around the peptide in water is mainly due to the strong interactions of PEG with charged residues, especially Lys, and hydrophobic residues, especially Ala. These results are analogous to previous studies on proteins which showed that mechanical stability of proteins can be improved by protecting their key load-bearing hydrogen bonds from water attacks by means of burying them in a hydrophobic core.[60,61] Our study illustrates that the mechanism through which PEG conjugation stabilizes α-helices is similar. This strategy could thus be used to design and fabricate new hybrid biomolecular nanomaterials with diverse capabilities and functionalities.

It should be noted that the solvent selection could significantly affect peptide−PEG interactions. Our CG simulations of peptide−PEG conjugates in different solvents suggest that as the solvent becomes more hydrophobic, the hydrophobic domains of peptide become more exposed to solvent and this makes PEG interact more with the hydrophilic regions of the peptide. This trend could be utilized to create solvent-responsive conformational changes in hierarchical peptide assemblies such as coiled coils.[62]

Our simulations show that PEG conjugation increases the stability of an α-helix by decreasing its solvent accessible surface area. The mechanistic finding that peptide SASA can be modulated significantly by side-chain conjugation as well as the solvent environment opens up possibilities for future mechanistic studies on peptide−polymer−solvent interactions and synthesis efforts that can capitulate on this finding to promote stable proteins, hierarchical assemblies, and nanoscale constructs with diverse functionalities.

ASSOCIATED CONTENT

Supporting Information

The all-atom and coarse-grained results for radius of gyration of PEG of different molecular weights in water are listed and compared in Table S1. Distribution of PEG monomers along the axis of helix for different PEG molecular weights is included. A movie showing the conformation dynamics of PEG around the helix is also provided. This material is available free of charge via the Internet at http://pubs.acs.org.

AUTHOR INFORMATION

Corresponding Author

*E-mail: s-keten@northwestern.edu.

Notes

The authors declare no competing financial interest.

ACKNOWLEDGMENTS

The authors acknowledge funding from the National Science Foundation (Award No. CBET-1234305) and the Office of Naval Research (Grant No. N00014-13-1-0760). S.K. and E.H. further acknowledge funding by a Booster Award from the Initiative for Sustainability and Energy (ISEN) at Northwestern University and an ASME Applied Mechanics Division Haythornthwaite Research Initiation Grant. The authors further acknowledge support from the Departments of Civil and Environmental Engineering and Mechanical Engineering at Northwestern University, as well as a supercomputing grant from Northwestern University High Performance Computing Center.

REFERENCES

(1) Pauling, L.; Corey, R. B.; Branson, H. R. *Proc. Natl. Acad. Sci. U.S.A.* **1951**, *37*, 205−211.
(2) Boerner, H. G.; Schlaad, H. *Soft Matter* **2007**, *3*, 394−408.
(3) Gabrielson, N. P.; Lu, H.; Yin, L.; Li, D.; Wang, F.; Cheng, J. *Angew. Chem., Int. Ed.* **2012**, *51*, 1143−1147.
(4) Holowka, E. P.; Pochan, D. J.; Deming, T. J. *J. Am. Chem. Soc.* **2005**, *127*, 12423−12428.
(5) Nowak, A. P.; Breedveld, V.; Pakstis, L.; Ozbas, B.; Pine, D. J.; Pochan, D.; Deming, T. J. *Nature* **2002**, *417*, 424−428.
(6) Petka, W. A.; Harden, J. L.; McGrath, K. P.; Wirtz, D.; Tirrell, D. A. *Science* **1998**, *281*, 389−392.
(7) Yu, Y. B. *Adv. Drug Delivery Rev.* **2002**, *54*, 1113−1129.
(8) Mahler, H.-C.; Friess, W.; Grauschopf, U.; Kiese, S. *J. Pharm. Sci.* **2009**, *98*, 2909−2934.
(9) Sanchez-Ruiz, J. M. *Biophys. Chem.* **2010**, *148*, 1−15.
(10) Sheparovych, R.; Roiter, Y.; Yang, J.; Kopecek, J.; Minko, S. *Biomacromolecules* **2009**, *10*, 1955−1961.
(11) Uversky, V. N.; Li, J.; Fink, A. L. *J. Biol. Chem.* **2001**, *276*, 10737−10744.
(12) Xu, C.; Kopecek, J. *Pharm. Res.* **2008**, *25*, 674−682.

(13) Bilgicer, B.; Fichera, A.; Kumar, K. *J. Am. Chem. Soc.* **2001**, *123*, 4393−4399.
(14) Tang, Y.; Ghirlanda, G.; Petka, W. A.; Nakajima, T.; DeGrado, W. F.; Tirrell, D. A. *Angew. Chem., Int. Ed.* **2001**, *40*, 1494−1496.
(15) Tang, Y.; Ghirlanda, G.; Vaidehi, N.; Kua, J.; Mainz, D. T.; Goddard, W. A.; DeGrado, W. F.; Tirrell, D. A. *Biochemistry* **2001**, *40*, 2790−2796.
(16) Austin, R. E.; Maplestone, R. A.; Sefler, A. M.; Liu, K.; Hruzewicz, W. N.; Liu, C. W.; Cho, H. S.; Wemmer, D. E.; Bartlett, P. A. *J. Am. Chem. Soc.* **1997**, *119*, 6461−6472.
(17) Chakrabartty, A.; Doig, A. J.; Baldwin, R. L. *Proc. Natl. Acad. Sci. U.S.A.* **1993**, *90*, 11332−11336.
(18) Patgiri, A.; Jochim, A. L.; Arora, P. S. *Acc. Chem. Res.* **2008**, *41*, 1289−1300.
(19) Patgiri, A.; Menzenski, M. Z.; Mahon, A. B.; Arora, P. S. *Nat. Protoc.* **2010**, *5*, 1857−1865.
(20) Blackwell, H. E.; Grubbs, R. H. *Angew. Chem., Int. Ed.* **1998**, *37*, 3281−3284.
(21) Kutchukian, P. S.; Yang, J. S.; Verdine, G. L.; Shakhnovich, E. I. *J. Am. Chem. Soc.* **2009**, *131*, 4622−4627.
(22) Schafmeister, C. E.; Po, J.; Verdine, G. L. *J. Am. Chem. Soc.* **2000**, *122*, 5891−5892.
(23) Krylov, D.; Barchi, J.; Vinson, C. *J. Mol. Biol.* **1998**, *279*, 959−972.
(24) Mayne, L.; Englander, S. W.; Qiu, R.; Yang, J. X.; Gong, Y. X.; Spek, E. J.; Kallenbach, N. R. *J. Am. Chem. Soc.* **1998**, *120*, 10643−10645.
(25) Zhou, N. E.; Kay, C. M.; Hodges, R. S. *J. Mol. Biol.* **1994**, *237*, 500−512.
(26) Andrews, M. J. I.; Tabor, A. B. *Tetrahedron* **1999**, *55*, 11711−11743.
(27) Houston, M. E.; Campbell, A. P.; Lix, B.; Kay, C. M.; Sykes, B. D.; Hodges, R. S. *Biochemistry* **1996**, *35*, 10041−10050.
(28) Osapay, G.; Taylor, J. W. *J. Am. Chem. Soc.* **1990**, *112*, 6046−6051.
(29) Taylor, J. W. *Biopolymers* **2002**, *66*, 49−75.
(30) Hodges, R. S.; Zhou, N. E.; Kay, C. M.; Semchuk, P. D. *Pept. Res.* **1990**, *3*, 123−137.
(31) Pellegrini, M.; Royo, M.; Chorev, M.; Mierke, D. F. *J. Pept. Res.* **1997**, *49*, 404−414.
(32) Zhou, N. E.; Kay, C. M.; Hodges, R. S. *Biochemistry* **1993**, *32*, 3178−3187.
(33) Esser-Kahn, A. P.; Francis, M. B. *Angew. Chem., Int. Ed.* **2008**, *47*, 3751−3754.
(34) Rosler, A.; Klok, H. A.; Hamley, I. W.; Castelletto, V.; Mykhaylyk, O. O. *Biomacromolecules* **2003**, *4*, 859−863.
(35) Vandermeulen, G. W. M.; Tziatzios, C.; Duncan, R.; Klok, H. A. *Macromolecules* **2005**, *38*, 761−769.
(36) Shu, J. Y.; Panganiban, B.; Xu, T. *Annu. Rev. Phys. Chem.* **2013**, *64*, 631−657.
(37) Pechar, M.; Kopeckova, P.; Joss, L.; Kopecek, J. *Macromol. Biosci.* **2002**, *2*, 199−206.
(38) Vandermeulen, G. W. M.; Tziatzios, C.; Klok, H. A. *Macromolecules* **2003**, *36*, 4107−4114.
(39) Shu, J. Y.; Tan, C.; DeGrado, W. F.; Xu, T. *Biomacromolecules* **2008**, *9*, 2111−2117.
(40) Top, A.; Roberts, C. J.; Kiick, K. L. *Biomacromolecules* **2011**, *12*, 2184−2192.
(41) Jain, A.; Ashbaugh, H. S. *Biomacromolecules* **2011**, *12*, 2729−2734.
(42) Ogihara, N. L.; Weiss, M. S.; Degrado, W. F.; Eisenberg, D. *Protein Sci.* **1997**, *6*, 80−88.
(43) Phillips, J. C.; Braun, R.; Wang, W.; Gumbart, J.; Tajkhorshid, E.; Villa, E.; Chipot, C.; Skeel, R. D.; Kalé, L.; Schulten, K. *J. Comput. Chem.* **2005**, *26*, 1781−1802.
(44) Jorgensen, W. L.; Chandrasekhar, J.; Madura, J. D.; Impey, R. W.; Klein, M. L. *J. Chem. Phys.* **1983**, *79*, 926−935.
(45) Vanommeslaeghe, K.; Hatcher, E.; Acharya, C.; Kundu, S.; Zhong, S.; Shim, J.; Darian, E.; Guvench, O.; Lopes, P.; Vorobyov, I.; MacKerell, A. D., Jr. *J. Comput. Chem.* **2010**, *31*, 671−690.
(46) Humphrey, W.; Dalke, A.; Schulten, K. *J. Mol. Graphics* **1996**, *14*, 33−38.
(47) Marrink, S. J.; de Vries, A. H.; Mark, A. E. *J. Phys. Chem. B* **2004**, *108*, 750−760.
(48) Marrink, S. J.; Risselada, H. J.; Yefimov, S.; Tieleman, D. P.; de Vries, A. H. *J. Phys. Chem. B* **2007**, *111*, 7812−7824.
(49) Lee, H.; de Vries, A. H.; Marrink, S.-J.; Pastor, R. W. *J. Phys. Chem. B* **2009**, *113*, 13186−13194.
(50) Chiu, S.-W.; Scott, H. L.; Jakobsson, E. *J. Chem. Theory Comput.* **2010**, *6*, 851−863.
(51) Stroberg, W.; Keten, S.; Liu, W. K. *Langmuir* **2012**, *28*, 14488−14495.
(52) Kuga, S. *J. Chromatogr.* **1981**, *206*, 449−461.
(53) Shu, J. Y.; Lund, R.; Xu, T. *Biomacromolecules* **2012**, *13*, 1945−1955.
(54) Cammas, S.; Harada, A.; Nagasaki, Y.; Kataoka, K. *Macromolecules* **1996**, *29*, 3227−3231.
(55) Harada, A.; Cammas, S.; Kataoka, K. *Macromolecules* **1996**, *29*, 6183−6188.
(56) Hourani, R.; Zhang, C.; van der Weegen, R.; Ruiz, L.; Li, C.; Keten, S.; Helms, B. A.; Xu, T. *J. Am. Chem. Soc.* **2011**, *133*, 15296−15299.
(57) Vandermeulen, G. W. M.; Klok, H. A. *Macromol. Biosci.* **2004**, *4*, 383−398.
(58) Xu, T.; Zhao, N.; Ren, F.; Hourani, R.; Lee, M. T.; Shu, J. Y.; Mao, S.; Helms, B. A. *ACS Nano* **2011**, *5*, 1376−1384.
(59) Xue, Y.; O'Mara, M. L.; Surawski, P. P.; Trau, M.; Mark, A. E. *Langmuir* **2011**, *27*, 296−303.
(60) Guzman, D. L.; Randall, A.; Baldi, P.; Guan, Z. *Proc. Natl. Acad. Sci. U.S.A.* **2010**, *107*, 1989−1994.
(61) Kushner, A. M.; Guan, Z. *Angew. Chem., Int. Ed.* **2011**, *50*, 9026−9057.
(62) Dube, N.; Presley, A. D.; Shu, J. Y.; Xu, T. *Macromol. Rapid Commun.* **2011**, *32*, 344−353.